# A novel image enhancement method for palm vein images

Kaveen Perera, Fouad Khelifi, Ammar Belatreche

***Abstract*— Palm vein images usually suffer from low contrast due to skin surface scattering the radiance of NIR light and image sensor limitations, hence require employing various techniques to enhance the contrast of the image prior to feature extraction. This paper presents a novel image enhancement method referred to as Multiple Overlapping Tiles (MOT) which adaptively stretches the local contrast of palm vein images using multiple layers of overlapping image tiles. The experiments conducted on the CASIA palm vein image dataset demonstrate that the MOT method retains the finer subspace details of vein images which allows excellent feature detection and matching with SIFT and RootSIFT features. Results on existing palm vein recognition systems demonstrate that the proposed MOT method delivers lower EER values outperforming other existing palm vein image enhancement methods.**

## I. Introduction

Conventional authentication methods such as pin codes and passwords are long proved to be inefficient and insecure. Biometrics provides much more secure recognition methods using one or more physiological traits [1]. Vascular biometrics recognition systems use the patterns of blood vessels under the skin to determine the identity of an individual. These vessel networks of every individual are different, even between identical twins. These patterns do not change significantly over time, which increases the security and reliability of a palm vein recognition system. Further, palm vein images can provide a greater degree of distinctive features with richer texture information.

Contactless palm vein based recognition systems are non-invasive and hygienic, making them more user-friendly than other biometrics recognition methods which boost their user acceptance [2]. Near-Infrared Light (NIR Light) penetrates the skin tissues and the deoxidised veins close to the skin surface absorb NIR light making them appear darker on images. However, the skin tissues scatter the radiance of NIR light causing the vein patterns to appear blurry and images to be in poor contrast. When combined with image sensor noise of capture devices, feature extraction and other subsequent processing on these low contrast images are very challenging. Therefore, a contrast enhancement pre-processing operation is required prior to employing any feature extraction algorithm.

The most commonly used image enhancement technique in palm vein recognition is Contrast Limited Adaptive Histogram Equalization (CLAHE) [3] followed by Histogram equalization (HE) [4] and adaptive histogram equalization (AHE) [5]. CLAHE is used in many applications with a lower tile count and clip values in single digits. A major problem identified with CLAHE is that when increasing the tile count and clip values to enhance the image contrast, a grid pattern starts to appear (*Fig. 1[e-f]*), thus making the images unsuitable for feature extraction. A number of observations have been made on the Scale-Invariant Feature Transform (SIFT) features extracted using HE, AHE and CLAHE enhancement techniques. While CLAHE produces a better local contrast distribution in comparison to HE and AHE. HE

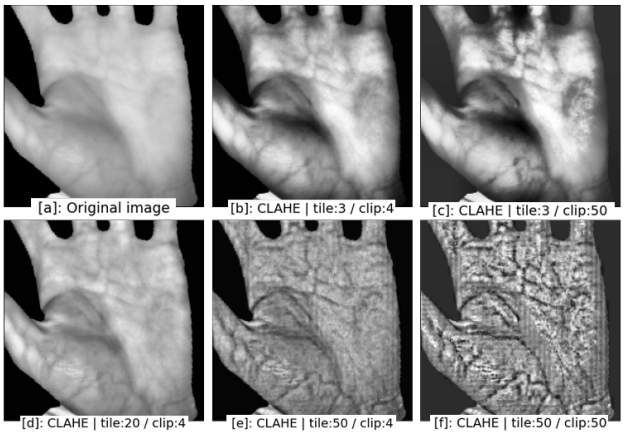


Figure 1. CLAHE with various tile counts and clip values. A higher tile count produces a grid pattern while enhancing the visibility of vein pattern.

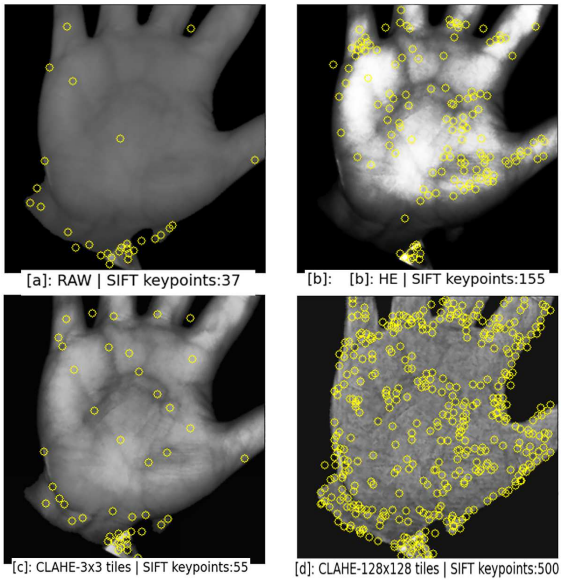


Figure 2. Comparison of SIFT features on Raw, HE and CLAHE enhanced images. Maximum SIFT keypoints were limited to 500.

The Authors are with the Computer & Information Sciences department of University of Northumbria at Newcastle, United Kingdom. Email: {kaveen.perera, fouad.khelifi, ammar.belatreche} @northumbria.ac.uk

clips out most of the details of the vein image and does not detect a significant number of SIFT features (*Fig. 2 [b]*). CLAHE with a lower tile count did not produce a sufficient number of SIFT features (*Fig. 2[c]*), but with a higher tile count SIFT features were mostly detected towards the edges of the palm (*Fig. 2[d]*). HE clipped out most of the details of the image while AHE produced intermediary results which are poorer than with CLAHE.

To address these issues identified with existing image enhancement methods on palm vein images, we propose a novel contrast enhancement method, which significantly boosts feature detection in the center area of the palm. We start by subdividing an image into smaller tiles, then stretching the contrast of each tile and applying a radial transparency mask. We repeat this process on three more layers of image tiles to overlap the edges and the vertices of the base tiles layer and sum the 4 layers together to produce the final contrast enhanced image. This method is referred to as Multiple Overlapping Tiles (MOT). We further test the performance of the proposed enhancement method using existing SIFT and RootSIFT based palm vein recognition systems [6]–[9]. In section III *Fig. 3* we present a workflow of the proposed image enhancement method.

The rest of the paper is organized as follows. In Section II we present a review of existing vein image enhancement methods. Section III discusses the proposed method and Section IV discusses the obtained experimental results. Finally, Section V draws conclusions and provides recommendations for further developments and enhancements of the proposed approach.

## II. . Related Work

Previous research has employed various techniques to enhance the contrast of vein images. Zhou and Kumar [10] estimated the background intensities profile, by subdividing the image into 32x32 size image tiles. As a measure to address the blocky effect these image tiles overlap each other by 3 pixels. Then the average grey level of each block is computed to estimate the respective background profile, which is then scaled to match the original image using bicubic interpolation and subtracted from the original image. Then HE is applied to enhance the vein image. Lee [11] employed a similar technique which subdivides the image into 16x16 non overlapping tiles prior to calculating average grayscale values for each tile. However, they do not use HE as in [10]. Soh et al [7] proposed an image enhancement process applying a CLAHE operation and then stretching histograms of 8x8 image blocks. A common issue with these techniques is the blocky effect rendered at the edges of the image tiles. [7] and [11] do not address the blocky effect at all while the 3 pixel overlapping used in [10] is not sufficient to address the blocky effect. Further, using HE can clip out details of the image.

Yang and Zhang [12] worked upon the concepts of image dehazing techniques (which are used to remove scattered light effect on foggy images to improve backgrounds visibility), and introduced a new technique to reduce light scatter caused by skin tissues as a vein image enhancement method. Yang and Yang [13] proposed a multi-channel Gabor filter based vein pattern enhancement method. Gabor filter parameters are automatically determined based on the width and orientation of vein networks hence the 4-orientations even-symmetric Gabor filter channels have different center frequencies. Then the four images are fused to produce the final enhanced image. Kim [14] propose an image smoothing technique by accounting the intensity change speed or rate. The speed of intensity change of flat areas where no vein patterns occur are slower than in the areas with vein patterns. The intensity difference between the original image and a smoothed version which is referred to as smoothing speed has been used to differentiate vein patterns from the background. A common issue observed with [12] [13] [14] is that these image smoothing techniques discard vital subspace information which can be used to detect robust features.

Trabelsi et al [15] calculated the global mean grey and variance values, then used a convolutional kernel which take the global mean and variance along with an enhancement constant into account to calculate the local response. This method introduces a darkening effect in areas where vein patterns branch out or occur very closely to each other and amplify the noise level which would require further filtering.

Van et al [6] proposed a Local Binary Patterns (LBP) based image enhancement method. They improved Center Symmetric LBP (CS-LBP) to propose a new method referred to as Enhanced CS-LBP (ECS-LBP). They compared their image enhancement method against Gabor filters, LBP, CS-LPB. These LBP based image enhancement methods clip out and discard most of the subspace information which makes them unsuitable to use with invariant features. Yan et al [9] discussed an image sharpening technique which they first multiply the image with an enhancement factor of 10, and then filtering the resulting image with the Prewitt high pass operator. This is then subtracted from the original image. Kang et al [16] introduced a Difference of Gaussian filters (DoG) and histogram equalization based method. A DoG filter with 4:1 Gaussian kernels ratio has been used as a band-pass filter to discard high frequencies. Then HE is applied to the DoG filtered image. This method is referred to as DoG-HE. Similar to the issues discussed with other methods these techniques discard subspace information making them unsuitable for feature extraction.

## III. THE PROPOSED METHOD

### A. Adaptive Contrast Stretch

The core concept of the proposed method is referred to as Adaptive Contrast Stretch (ACS). Contrast stretch is also referred to as pixel normalization [17]. The ACS method subdivides an image into N sized square shaped tiles, and then (1) is used to stretch and scale the histogram of each tile within the range of available intensities or grey levels.

$$F_{TN} = \left( \frac{T_{Ni} - \min(T_N)}{\max(T_N) - \min(T_N)} \right) \times 255 \quad (1)$$

In (1), an image tile is denoted as $T$ and $T_N$ is an $NxN$ sized block of pixels in the image, while $i$ represents a pixel in that tile. $\min(T_N)$ and $\max(T_N)$ are the minimum and maximum

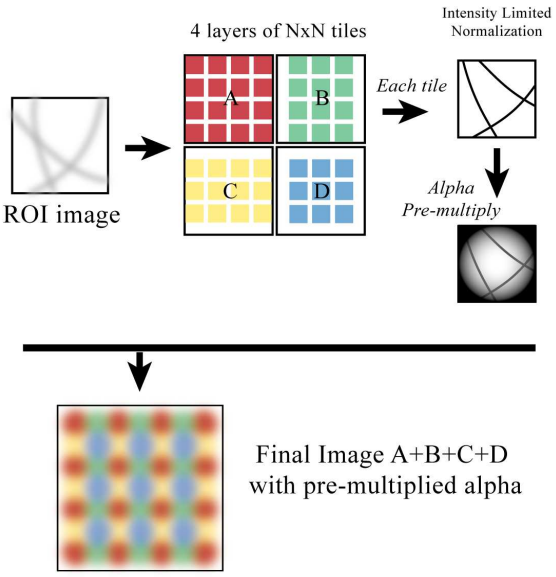


Figure 3. Workflow chart of the proposed image enhancement method. In the 4 layers of NxN, A – initial image tiles, B – Vertical overlaps, C – Horizontal overlaps, D – Common vertex overlaps (Gaps between the tiles added for visual clarity and illustrative purposes only)

pixel values of a selected tile. Should the range of pixel values within a tile evaluates to 0 the value of the denominator in (1) ($\max(T_N) - \min(T_N)$) is set to 1 to avoid 'division by zero'. As palm vein images are provided as 8-bit images the output is multiplied by 255. The generation of an ACS image involves the following steps: (i) find the minimum and maximum pixel values of the image tile, (ii) apply (1) for to each pixel in that image tile, and then repeat all the above steps for all the image tiles. To assess performance against the tile size we experimented with *NxN* sized tiles ranging from 2 to 32. To simplify calculations, we only used even numbered tile sizes. Most of the details of a low contrast palm image is concentrated in the mid-range of the histogram (*Fig. 4[a]*). A potential issue observed is that when this histogram is stretched some of the finer details are clipped out as most of the details are now remapped to very bright intensities and are concentrated towards the high end of the histogram (*Fig. 4[b]*). This effect is very noticeable on larger tile sizes.

To address this clipping issue, the multiplying factor of (1) is applied with a floor function. The mathematical notation for the modified formula is presented on (2). This method is referred to as 'Intensity Limited Normalization' (ILN). ILN is used for the rest of the ACS based image enhancements of the remainder of this paper.

$$F_{TN} = \left( T_{Ni} - \min(T_N) \right) \times \left\lfloor \frac{255}{\max(T_N) - \min(T_N)} \right\rfloor \qquad (2)$$

We can observe from *Fig. 4[c]* that when Intensity Limited Normalization is applied, new pixel values have an even distribution and no longer concentrate towards the brighter/high end of the histogram. However, ACS generated a blocky artifact at the edges of each image tile (*Fig. 5[b-c]*). These artifacts are produced because the pixel values have been remapped based only on the minimum and maximum

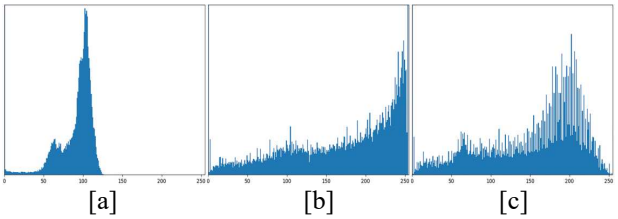


Figure 4. Histogram of a sample tile [a] before and [b] after applying ACS. [c] After applying ACS with Intensity Limited Normalization. The heights of the histograms are not equal and scaled to fit into the page layout.

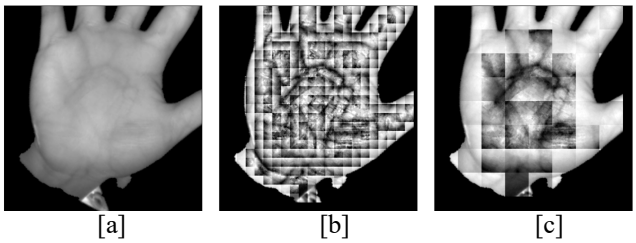


Figure 5. [a] original palm image, [b] ACS with N=12 tile size, [c] ACS with N=32 tile size.

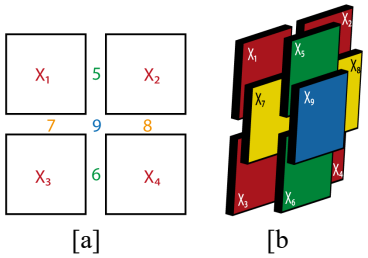


Figure 6. [a] Examination of 4 neighbouring tiles. [b] Overlapping tiles used for MOT method.

pixel values of that respective tile, which disregard the intensities of the neighboring tiles. As a result, two adjacent pixels from neighboring image tiles with minimal grayscale value differences between them, could be remapped to very distinctive values.

### *B. Multiple Overlapping Tiles (MOT)*

To address the blocky effect, we examined 4 neighboring tiles $X_1$-$X_4$ in *Fig. 6[a]*. 5, 6 are vertical edges and 7, 8 are the horizontal edges while 9 is the common vertex across all the 4 tiles. We created overlapping ACS image tiles at the edges ($X_5$-$X_6$ and $X_7$-$X_8$ in *Fig. 6[b]*) and the common vertex ($X_9$ in *Fig. 6[b]*) and averaged them with the initial ACS image layer. To apply this to the entire image, 3 more overlapping layers were created. *Fig. 3* illustrates all 4 layers of overlapping tiles named A, B, C and D, where the tiles of the second and the third layers (B, C) center the respective vertical and horizontal edges of the base tiles layer (A), and the tiles in forth layer (D) center the common vertices of the base tiles layer. However, after this step a lesser contrast edge (or a shallow blocky effect) was still visible (*Fig. 8[a]*). To further suppress the blocky effect, we added a radial opacity decay to each tile from the center towards the edges. To generate the final image the sum of all 4 layers is used. This method is referred to as the Multiple Overlapping Tiles (MOT). The radial decay effect can be achieved using a

Figure 7. Radial decay effect created using a 2D Guassian

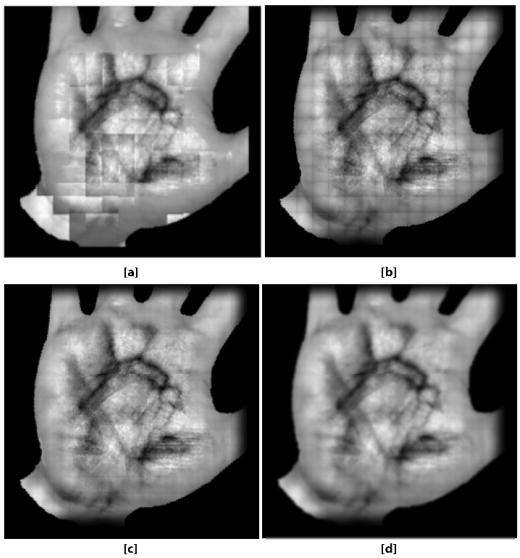


Figure 8. [a] After suming up overallping edges and vetices tile lyares. [b] Using an incorrect σ for MOT. [c] Using N/4.4 for MOT. [d] Final smoothed MOT image.

grayscale radial gradient as a transparency mask (*Fig. 7*). Such a gradient can be generated with a 2D isotropic Gaussian function in (3). Equation (3) is also used to create low-pass filters for image smoothing/blurring. However, in the MOT method, it is only used to create a transparency mask which is also referred to as an alpha channel (α). A 2D isotropic Gaussian is generated from a mathematical function. Hence it is independent of any image or dataset. x and y in (3) are the width and height of an image tile and σ is the standard deviation. σ is used to control the slope (or the falloff) of the gaussian distribution to scale up/down the radial decay of the Gaussian mask.

$$G(x,y) = \frac{1}{2\pi\sigma^2} e^{-\frac{x^2+y^2}{2\sigma^2}} \quad (3)$$

Equation (4) is used to blend an image $f$ using a greyscale alpha channel α over a background image $b$ to create a new image $I_N$. This is also referred to as the over operator [18]. This formula assumes the background to be a solid image without an alpha channel.

$$I_N = [(1-\alpha)\, b] + \alpha\, f \quad (4)$$

This can also be efficiently computed as in (5). To preview an image with the alpha channel applied we can start with a black background matte (a 2D matrix with all the pixel values set to 0) and use (5) to overlay the image as the foreground.

$$I_N = b + \alpha(f - b) \quad (5)$$

When the background is equal to 0, (5) over operator can be reformulated as (6).

$$I_P = \alpha\, b \quad (6)$$

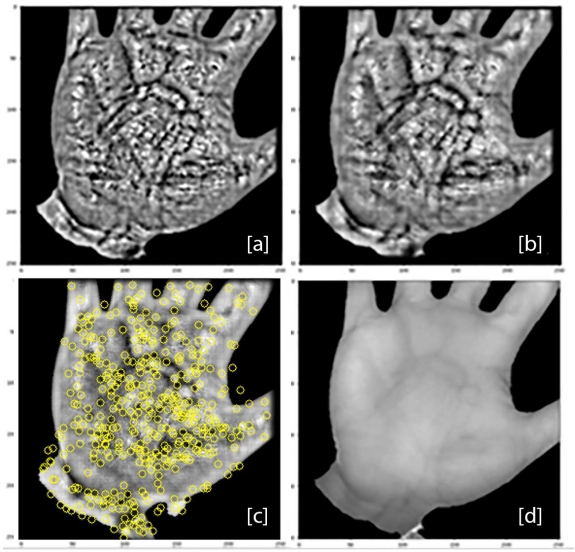


Figure 9. [a-b] MOT images of different tile sizes (N) 8, 12, pixels respectively. [c] MOT method with N=16, 500 SIFT features which are mostly concentrated in the centre area of the plam were detected. Maximum SIFT keypoints were limited to 500. [d] original image.

This is referred to as pre-multiplying in computer graphics and digital image composting. In (6) IP is the alpha pre-multiplied image.

To create the final image the 4 alpha pre-multiplied image layers are summed up. Incorrect values for σ in (3) can introduce a visible edge (Fig. 8[b]). The optimal value determined for σ to control the fall-off of the Gaussian masks is N/4.4 for any tile size between 8-32 pixels (Fig. 8[c]). However, artifacts can occur when using larger tile sizes. Finally, to smoothen the resulting MOT image a Gaussian blur was applied (Fig. 8[d]). Fig. 9[a-b] presents the final image enhanced with the proposed MOT method using different tile sizes. From Fig. 9[c] we can observe that when using MOT as the image enhancement method most of the SIFT features are detected in the center area of the palm.

## IV. EXPERIMENTS AND RESULTS

For this research the publicly available dataset CASIA[19] was used. The CASIA Multi Spectral dataset contains 6 images per left and right hands, with varying orientations and stretch levels (of fingers and thumb) captured from 100 participants. Images were captured under 460nm, 630nm, 700nm, 850nm, 940nm and white lights. A total of 1200 images are available per each wavelength in JPEG format. Image sensor noise and artifacts introduced by lossy JPEG compression are presented in all the images. The dataset does not contain any palm images with visible scars or other skin damage. Best contrast on vein images is recorded when the wavelength is between 820nm-880nm [20]. Therefore, experiments were carried out on the 850nm subset of the CASIA multi-spectral dataset in the 1:m (1 to many) closed set approach. The CASIA dataset was split into 20% (240 images) for training and 80% (960 images) for testing. To maximize the number of samples left and right hands from a single subject were used as two separate subjects, except

opposite palms of a particular subject were not matched against each other.

We used the entire palm as the ROI. The convex-hull method described in [21] was used to identify the thumb and finger tips of a palm image, while image contours and thresholding were used to extract a binary matte of the palm and used with an erosion filter to use as a mask to filter out the feature points reside closer to the edges. This method produces variable sized ROI images. All the images were scaled down to 60% from the original image size prior to any processing.

To assess the proposed image enhancement method, several palm-vein image recognition systems which use SIFT and RootSIFT features with the CASIA dataset have been implemented. With the SIFT features we applied Euclidian Distance (ED) [6] [8] [9], ED then RANSAC filtering [7]. With the RootSIFT features we applied k-nearest neighbors algorithm (KNN) along with distance ratio test (RT) and bidirectional matching methods presented in [8]. We replaced the pre-processing stage in these systems with the proposed MOT method and verified the resulting performance.

In [8], DoG-HE is used to enhance the image and extract SIFT and RootSIFT features. In this experiment, they have used their own dataset as well as all the images from 700nm, 850nm, and 940nm subsets of the CASIA multispectral dataset. In the 850nm CASIA subset based experiment, 3 images were used as reference images and have used 3 intra class and 6 inter class query images. In [7] the image was first applied with CLAHE and then used histogram stretching on image blocks to enhance the image prior to feature extraction with SIFT. The SIFT features were first matched using the ED then mismatches were estimated with RANSAC algorithm. In [6], ECS-LBP is applied prior to extracting and matching SIFT features using ED and matching between left and right hands was separated. In [9] a Prewitt high pass filter was used to enhance the images before extracting SIFT and ORB features. Features are then matched using ED bidirectionally between the template and probe images. They further present results with several multi feature score fusion algorithms. However, we implemented their bidirectional matching method only with SIFT features.

The aforementioned recognition systems have not discussed the used parameter values in their experiments except in [8] where it was reported that a threshold of 0.8 has been used for RT. To determine the optimal tile size ($N$) for SIFT and RootSIFT feature matching which yield best true positive (TP) and true negative (TN) rates, we experimented with tile sizes from 12, 16, 20, 24, 28, 32, 36. The greatest difference between TP and TN was observed when the image tile size is 12 pixels closely followed by 16. To improve the computational time, we used 16x16 image tiles for all the experiments. The corresponding results are shown in Table I where the Equal Error Rate (EER) has been used as a measure of assessment. Our proposed method reduce the EER values when using SIFT based matching methods proposed by [8], [7]. The recognition methods involving RANSAC filtering were computed with a significant increase in the computational time. Using the RootSIFT features our proposed method reduces the EER values when using ED based matching.

TABLE I. PERFORMANCE COMPARISON WITH EXISTING PALM VEIN RECOGNITION SYSTEMS. THE EXPERIMENTAL RESULTS ARE PRESENTED USING 1 REGISTRATION IMAGE UNLESS OTHERWISE NOTED.

| **Recognition technique** | EER % |
|---|---|
| Multiply + Prewitt filter + SIFT (ED + bidirectional matching) [9] | 1.84 |
| **MOT + SIFT (ED + bidirectional matching)** | 7.769 |
| Dog-HE + SIFT (ED) [8] (3 registration images) | (Left hand) 2.87 |
| **MOT + SIFT (ED)** (3 registration images) | (Left hand) **1.478** |
| CLAHE + block stretch + SIFT (ED + RANSAC) [7] | 14.7 |
| **MOT + block stretch + SIFT (ED + RANSAC)** | **4.292** |
| GABOR + SIFT (ED) [6] | (L/R hands) 3.65/3.82 |
| CS-LBP + SIFT (ED) [6] | (L/R hands) 4.51/4.78 |
| ECS-LBP + SIFT (ED) [6] | (L/R hands) 3.12/3.25 |
| **MOT + SIFT (ED)** | (L/R hands) **2.75/2.876** |
| DoG-HE + RootSIFT (ED) [8] (3 registration images) | (Left hand) 2.16 |
| **MOT + RootSIFT (ED)** (3 registration images) | (Left hand) **1.266** |
| DoG-HE + RootSIFT (KNN + RT + Bidirectional matching) [8] (3 registration images) | (Left hand) 0.16 |
| **MOT + RootSIFT (KNN + RT + Bidirectional matching)** (3 registration images) | (Left hand) **0.401** |

TABLE II. EER % VALUES WITH SIFT, 1-5 REGISTRATION IMAGES

| **Registration images** | **ED** | **ED + RANSAC** | **KNN+RT** | **KNN+RT+ RANSAC** |
|---|---|---|---|---|
| 1 | 3.333 | 4.292 | 2.873 | 4.967 |
| 2 | 1.677 | 3.212 | 1.725 | 3.023 |
| 3 | 1.715 | 2.9 | 1.663 | 1.867 |
| 4 | 0.53 | 1.297 | 0.61 | 1.125 |
| **5** | **0.31** | **0.638** | **0.278** | **0.573** |

TABLE III. EER % VALUES WITH ROOTSIFT, 1-5 REGISTRATION IMAGES (REFERRED TO AS REG # IN COLUMN 1)

| **Reg. #** | **ED** | **ED + RANSAC** | **KNN+ RT** | **KNN+RT+ RANSAC** | **KNN+RT + Bidirectional** |
|---|---|---|---|---|---|
| 1 | 1.982 | 5.657 | 2.528 | 5.394 | 2.505 |
| 2 | 1.259 | 3.828 | 1.707 | 2.582 | 0.893 |
| 3 | 1.423 | 3.799 | 1.16 | 2.218 | 0.647 |
| 4 | 0.588 | 1.547 | 0.506 | 1.16 | 0.315 |
| **5** | **0.342** | **1.284** | **0.262** | **0.62** | **0.101** |

Further [6] present separate EER values for left and right hands. They only match left hands with other left hands and right hands with other right hands. This reduces the total number of inter class matching by half. Our experiments with separate left/right hands matching indicated that reducing the total number of inter class matches causes a significant drop of EER values. Our experiments with bidirectional matching methods on SIFT [9] and RootSIFT [8] resulted in higher EER values than the original research. Especially the EER value difference is significantly high against [9]. However, the EER values from our experiments of the corresponding forward matching methods (SIFT+ED in [9] and SIFT+ED, RootSIFT+ED in [8]) are lower than of the original research, which they have produced forward matching results using the same image enhancement method as of the bidirectional method. This confirms that our image enhancement method outperforms all the other compared enhancement methods.

We further tested our approach using 1-5 registration images using ED, ED+RANSAC, KNN+RT, KNN+RT+RANSAC with both SIFT and RootSIFT. For RT with the above-mentioned method, we used a threshold of 0.7 [22]. Additionally, with SIFT ED+Bidirectional matching and with RootSIFT KNN+RT+ Bidirectional matching was performed with a RT threshold of 0.8 [8]. These results are presented in Table II and Table III. With every additional registration image, EER values are reduced for all the methods except for ED matching with 3 registration images. ED method performed slightly better with SIFT when using 4-5 registration images. RANSAC based methods (ED+RANSAC and KNN+RT+RANSAC) performed better on with SIFT features. However, ED alone produced lower EER values than when using ED+RANSAC method. All the other methods performed better with RootSIFT features. Lowest EER values are recorded when using RootSIFT features with KNN+RT+Bidirectional method (0.101%) followed by KNN+RT method (0.262%).

## V. Conclusion

Palm vein images are inherently low contrast due to skin surface scattering of NIR light and image senor limitations. Current image enhancement methods discard finer details in the feature subspace either by clipping or smoothing out. We proposed a novel image enhancement method referred to as MOT to enhance low contrast palm vein images prior to feature extraction and further processing, while retaining these finer subspace details. The proposed MOT method is based on adaptive contrast stretching which subdivides an image into smaller image tiles and scale the contrast within the available intensities. For this purpose, we further introduced an intensity limited normalization method to prevent clipping details. The MOT method boosts the contrast of very fine details regardless of local illumination changes in different regions of an image. As a result, a higher number of SIFT features were detected in the center area of the palm. We applied the popular SIFT and RootSIFT based recognition methods to images enhanced using the proposed MOT method. Further experiments were carried out using a combination of methods with 1-5 registration images and the obtained results show that the proposed MOT method clearly outperforms other image enhancement methods. The use of MOT method can be extended to other closely related biometrics methods such as finger vein and palmprint. Furthermore, the proposed method can be further developed to enhance other types of dark or low contrast images.

## References


[1] D. Palma and P. L. Montessoro, *Biometric-Based Human Recognition Systems: An Overview*. IntechOpen, 2022. doi: 10.5772/intechopen.101686.

[2] A. K. Jain, A. Ross, and S. Prabhakar, 'An introduction to biometric recognition', *IEEE Transactions on Circuits and Systems for Video Technology*, vol. 14, no. 1, pp. 4–20, Jan. 2004, doi: 10.1109/TCSVT.2003.818349.

[3] P. Cancian, G. W. Di Donato, V. Rana, and M. D. Santambrogio, 'An embedded Gabor-based palm vein recognition system', in *2017 IEEE EMBS International Conference on Biomedical Health Informatics (BHI)*, Feb. 2017, pp. 405–408. doi: 10.1109/BHI.2017.7897291.

[4] A. Aglio-Caballero, B. Ríos-Sánchez, C. Sánchez-Ávila, and M. J. M. de Giles, 'Analysis of local binary patterns and uniform local binary patterns for palm vein biometric recognition', in *2017 International Carnahan Conference on Security Technology (ICCST)*, Oct. 2017, pp. 1–6. doi: 10.1109/CCST.2017.8167808.

[5] D. P. Gaikwad and S. P. Narote, 'Multi-modal biometric system using palm print and palm vein features', in *2013 Annual IEEE India Conference (INDICON)*, Dec. 2013, pp. 1–5. doi: 10.1109/INDCON.2013.6726010.

[6] H. T. Van, C. M. Duong, G. Van Vu, and T. H. Le, 'Palm Vein Recognition Using Enhanced Symmetry Local Binary Pattern and SIFT Features', in *2019 19th International Symposium on Communications and Information Technologies (ISCIT)*, Sep. 2019, pp. 311–316. doi: 10.1109/ISCIT.2019.8905179.

[7] S. C. Soh, M. Z. Ibrahim, M. B. Yakno, and D. J. Mulvaney, 'Palm Vein Recognition Using Scale Invariant Feature Transform with RANSAC Mismatching Removal', in *IT Convergence and Security 2017*, vol. 449, K. J. Kim, H. Kim, and N. Baek, Eds. Singapore: Springer Singapore, 2018, pp. 202–209. doi: 10.1007/978-981-10-6451-7_25.

[8] X. Yan, W. Kang, F. Deng, and Q. Wu, 'Palm vein recognition based on multi-sampling and feature-level fusion', *Neurocomputing*, vol. 151, pp. 798–807, Mar. 2015, doi: 10.1016/j.neucom.2014.10.019.

[9] X. Yan, F. Deng, and W. Kang, 'Palm Vein Recognition Based on Multi-algorithm and Score-Level Fusion', in *2014 Seventh International Symposium on Computational Intelligence and Design*, Dec. 2014, vol. 1, pp. 441–444. doi: 10.1109/ISCID.2014.93.

[10] Y. Zhou and A. Kumar, 'Human Identification Using Palm-Vein Images', *IEEE Transactions on Information Forensics and Security*, vol. 6, no. 4, Art. no. 4, Dec. 2011, doi: 10.1109/TIFS.2011.2158423.

[11] Y.-P. Lee, 'Palm vein recognition based on a modified (2D)2 LDA', *SIViP*, vol. 9, no. 1, pp. 229–242, Jan. 2015, doi: 10.1007/s11760-013-0425-6.

[12] J. Yang and B. Zhang, 'Scattering Removal for Finger-Vein Image Enhancement', in *2011 International Conference on Hand-Based Biometrics*, Nov. 2011, pp. 1–5. doi: 10.1109/ICHB.2011.6094321.

[13] J. Yang and J. Yang, 'Multi-Channel Gabor Filter Design for Finger-Vein Image Enhancement', in *2009 Fifth International Conference on Image and Graphics*, Sep. 2009, pp. 87–91. doi: 10.1109/ICIG.2009.170.

[14] W. Kim, 'Visibility Restoration via Smoothing Speed for Vein Recognition', *IEICE Trans. Inf. & Syst.*, vol. E102.D, no. 5, Art. no. 5, May 2019, doi: 10.1587/transinf.2018EDL8110.

[15] R. B. Trabelsi, A. Damak Masmoudi, and D. S. Masmoudi, 'A bi-modal palmvein palmprint biometric human identification based on fusing new CDSDP features', in *2015 International Conference on Advances in Biomedical Engineering (ICABME)*, Sep. 2015, pp. 1–4. doi: 10.1109/ICABME.2015.7323236.

[16] W. Kang, Y. Liu, Q. Wu, and X. Yue, 'Contact-Free Palm-Vein Recognition Based on Local Invariant Features', *PLOS ONE*, vol. 9, no. 5, Art. no. 5, May 2014, doi: 10.1371/journal.pone.0097548.

[17] I. T. Young, J. J. Gerbrands, and L. van Vliet, 'Fundamentals of image processing', in *The Digital Signal Processing Handbook*, V. K. Madisetti and D. B. Williams, Eds. CRC Press, 1998, p. 51.01-51.91.

[18] S. Dhanani and M. Parker, '7 - Alpha Blending', in *Digital Video Processing for Engineers*, S. Dhanani and M. Parker, Eds. Oxford: Newnes, 2013, pp. 49–52. doi: 10.1016/B978-0-12-415760-6.00007-6.

[19] Y. Hao, Z. Sun, and T. Tan, 'Comparative studies on multispectral palm image fusion for biometrics', in *Proceedings of the 8th Asian conference on Computer vision - Volume Part II*, Berlin, Heidelberg, Nov. 2007, pp. 12–21.

[20] A. Singh and D. Singh, 'Palm Vein Recognition Technology: A Literature Survey', *International Journal of Solid State Materials*, vol. 5, no. 1, Art. no. 1, Aug. 2019.

[21] W. L. Jhinn, M. G. K. Ong, L. S. Hoe, and T. Connie, 'Contactless Palm Vein ROI Extraction using Convex Hull Algorithm', in *Computational Science and Technology*, Singapore, 2019, pp. 25–35. doi: 10.1007/978-981-13-2622-6_3.

[22] D. G. Lowe, 'Distinctive Image Features from Scale-Invariant Keypoints', *International Journal of Computer Vision*, vol. 60, no. 2, Art. no. 2, Nov. 2004, doi: 10.1023/B:VISI.0000029664.99615.94.